Three-dielectric-layer hybrid solvation model with spheroidal cavities in biomolecular simulations

Changfeng Xue[1] and Shaozhong Deng[2,*]

[1]*Department of Fundamental Sciences, Yancheng Institute of Technology, Yancheng, Jiangsu 224003, People's Republic of China*

[2]*Department of Mathematics and Statistics, University of North Carolina at Charlotte, Charlotte, North Carolina 28223-0001, USA*

(Received 17 September 2009; published 5 January 2010)

This paper extends the three-dielectric-layer hybrid solvation model for treating electrostatic interactions in biomolecular simulations from the spherical geometry [Comm. Comp. Phys. **6**, 955 (2009)] to the prolate/oblate spheroidal geometries. In the resulting model, the inner spheroidal cavity of a low dielectric constant ε_i contains an irregular-shaped solute and some explicit solvent molecules, while the unbounded outer layer is used to implicitly model the bulk solvent as a dissimilar continuum medium of a high dielectric constant ε_o. The thin intermediate translation layer, which also consists of explicit solvent molecules, assumes a continuous variation of the dielectric permittivity $\varepsilon(\mathbf{r})$ changing smoothly from ε_i to ε_o. In particular, the so-called *quasiharmonic* dielectric permittivity profile is introduced based on a harmonic interpolation, thus allowing analytical series solutions of the generalized Coulomb potential and the self-polarization energy in terms of the associated Legendre functions. A key advantage of the proposed quasiharmonic dielectric model lies in the fact that it overcomes the inherent mathematical divergence in the self-polarization energy that exists in the simple and widely used steplike dielectric model. Numerical examples are included to show some simulated behaviors of the quasiharmonic dielectric model and the corresponding analytical solution.

DOI: 10.1103/PhysRevE.81.016701 PACS number(s): 02.70.−c, 82.20.Wt, 41.20.Cv, 73.21.La

I. INTRODUCTION

Electrostatic interactions are well known to provide crucial contributions to the structure, dynamics, and function of biomacromolecules; as such, they have been a subject of intense theoretical study in biomolecular simulations. Most electrostatic models applied in the computer simulation of a biomacromolecule adopt a full-atom representation of the macromolecule, but have the choice of treating the surrounding solvent as a collection of explicit solvent molecules or as an implicit continuum medium. Explicit representation of the solvent molecules [1–3] offers a detailed and accurate description of the biological system, yet all-atom simulations are expensive to perform due to the long-range nature of the electrostatic interactions. Alternatively, in implicit solvent models [4,5], a solvent is modeled as a continuum medium with a high dielectric constant outside the macromolecule, while the macromolecule atoms themselves are explicitly modeled with assigned partial charges embedded in a dissimilar continuum medium of a low dielectric constant inside the macromolecule volume. Although the neglect of explicit solvent molecules can significantly reduce the computational cost, the implicit solvent models also have fundamental limitations due to the fact that the important atomic details of how the solvent molecules interact with the surface of the macromolecule are ignored. In order to benefit the efficiency of implicit solvents for replacing the solvent that gives rise to much of the computational cost, while also directly model structural effects of the solvent in the proximity of the macromolecule, there has been considerable recent interest in developing hybrid explicit/implicit solvent models [6–8], in which the macromolecule together with a few boundary layers of the solvent molecules are considered explicitly within a dielectric cavity, and outside the cavity, the solvent is treated implicitly as a dielectric continuum.

In a hybrid solvent model, the shape of the dielectric cavity determines the amount of solvent to be treated explicitly around the solute. The spherical geometry has often been used because the electric field of a spherical dielectric object can be calculated analytically by the Kirkwood expansion [9] with arbitrary accuracy. However, this treatment may be inefficient for nonspherical solutes like certain globular proteins and other elongated biopolymers such as actin and DNA. For macromolecules of irregular shapes, using a corresponding irregular-shaped geometry to incorporate only a few shells of solvent molecules adjacent to the macromolecules would make the simulated system much smaller, but how to efficiently obtain an accurate electric field for such shapes remains a great challenge. In particular, to employ solvation shells with irregular shapes, the Poisson equation needs to be solved numerically at every simulation time step, which, depending on the system size, may become more computationally intensive than standard explicit all-atom solvent simulations. Therefore, for an irregular-shaped macromolecule, it may be more beneficial to adopt a nonspherical but still regular-shaped cavity that can conform closely to the irregular shape of the biomolecule. In the present paper, we focus on spheroidal cavities in particular, but it should be pointed out that, the results can be extended, in essence, in a straightforward manner to triaxial ellipsoidal cavities as well.

Generally speaking, we are concerned with accurate calculation of electrostatic interactions between charges inside a dielectric cavity immersed in an implicit solvent medium. For simplicity, in most theoretical studies of hybrid solvent models, macroscopic dielectric constants ε_i and ε_o are assigned for the cavity and the surrounding implicit medium, respectively, leading to a sharp jump in the dielectric constant at the interface between them. In this case, it is well known from classical electromagnetism that the presence of a charged particle inside the dielectric cavity polarizes the surrounding dissimilar dielectric medium, which in turn induces charges at the interface and makes a contribution, called the reaction field, to the electric field throughout the

*Corresponding author. shaodeng@uncc.edu

cavity. And accordingly, a new potential energy, usually called the self-polarization energy, arises due to the mutual interaction between the source charge and its own induced charges.

For the steplike dielectric model mentioned above, there exist analytical solutions for the electrostatic potential and the self-polarization energy [10–12], but unfortunately, there are a few disadvantages as well. By construction, all the induced charges will be localized at the cavity surface of zero width so that both the real and the induced charges can coincide at the same location, giving rise to a self-polarization energy that diverges at the cavity surface. Besides, at the cavity surface the sharp transition from ε_i to ε_o in the dielectric constant is clearly unphysical due to interdiffusion between the cavity and the surrounding medium. For spherical cavities, several solutions have been proposed to overcome the mathematical divergence of the steplike dielectric model, including the regularization method [13–15], and a more rigorous numerical approach [16,17] in which the steplike dielectric function is replaced by a continuous variation of the dielectric constant within a thin translation layer around the interface. We refer to any dielectric model of this kind as a three-layer model, the radial dielectric function $\varepsilon(\mathbf{r})$ changing smoothly from ε_i to ε_o within the translation layer. As a direct consequence of such a three-layer model, the induced charges are spread along the translation layer and the mathematical divergence in the self-polarization energy disappears. In fact, an explicit numerical formula for the self-polarization energy corresponding to general continuous three-layer dielectric models has been obtained [16]. However, as the numerical nature of this formula requires the discretization of the continuous dielectric function into a multistep (piecewise constant) one within the translation layer, new numerical divergence is encountered [18].

To overcome the inherent mathematical divergence of the steplike dielectric model, in Ref. [19], a novel three-dielectric-layer hybrid solvation model corresponding to the spherical geometry is introduced. In this model, the interior spherical cavity contains the solute and some explicit solvent molecules, while the exterior layer models the bulk solvent. In the intermediate layer that also contains explicit solvent molecules, a special dielectric permittivity profile, constructed through a harmonic interpolation, is employed to not only achieve a continuous transition from the interior cavity to the exterior layer but also allow an analytical series solution of the model by generalizing the Kirkwood series expansion. Therefore, the goal of the present paper is to extend the three-dielectric-layer hybrid solvation model from the spherical geometry to the prolate/oblate spheroidal geometries, and present the corresponding analytical series solutions. The paper is organized as follows. In Sec. II, we shall briefly review the analytical solution of the steplike model. Then in Sec. III, we will present the three-dielectric-layer hybrid solvation model with prolate spheroidal cavities, and the corresponding analytical solution. Next in Sec. IV, how to extend the results to oblate spheroidal cavities is briefly discussed. Numerical examples are then presented in Sec. V, and some concluding remarks are finally given in Sec. VI.

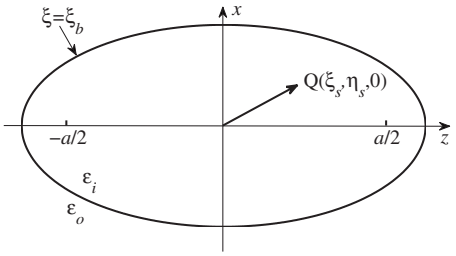

FIG. 1. Schematic illustration of the steplike dielectric model: the dielectric constants of a prolate spheroid and the surrounding medium are ε_i and ε_o, respectively. The prolate spheroid, defined by the equation $\xi=\xi_b$, has an interfocal distance a. A point charge e_s is located at the point $\mathbf{r}_s=(\xi_s,\eta_s,\phi_s=0)$ in the xz plane.

II. ANALYTICAL SOLUTION FOR THE STEPLIKE DIELECTRIC MODEL

Simply speaking, in the present paper we are concerned with the calculation of the generalized Coulomb potential energy between two particles inside or outside a dielectric prolate spheroid with the coordinates $\mathbf{r}$ and $\mathbf{r}_s$, and the charges e and e_s, respectively. First of all, there are several definitions of prolate spheroidal coordinates, and in this paper, the prolate spheroidal coordinates (ξ,η,ϕ) are defined in terms of the Cartesian ones (x,y,z) as follows:

$$x=\frac{a}{2}\sqrt{(\xi^2-1)(1-\eta^2)}\cos\,\phi,$$

$$y=\frac{a}{2}\sqrt{(\xi^2-1)(1-\eta^2)}\sin\,\phi,\quad z=\frac{a}{2}\xi\eta,$$

where a is the interfocal distance of the prolate spheroid, $\xi\in[1,\infty)$ is the radial variable, $\eta\in[-1,1]$ is the angular variable, and $\phi\in[0,2\pi]$ is the azimuthal variable, respectively. Note that the surface of constant ξ is a prolate spheroid with interfocal distance a ($\xi=1$ corresponds to the line between the foci). Also note that here the pole of the prolate spheroidal coordinate system is denoted by the z axis.

The generalized Coulomb potential energy between these two particles can be calculated through $V_c(\mathbf{r},\mathbf{r}_s)=e\Phi(\mathbf{r},\mathbf{r}_s)$, where $\Phi(\mathbf{r},\mathbf{r}_s)$ is the electrostatic potential which verifies the Poisson equation

$$\nabla\cdot\varepsilon(\mathbf{r})\,\nabla\,\Phi(\mathbf{r},\mathbf{r}_s)=-4\pi e_s\delta(\mathbf{r}-\mathbf{r}_s),\qquad(1)$$

where $\varepsilon(\mathbf{r})$ is the spatially dependent dielectric function, and $\delta(\ldots)$ is the Dirac delta function. The three-dimensional solution of this equation, even assuming the spheroidal geometry and only the radial ξ dependence for $\varepsilon(\mathbf{r})$, is quite complicated to find since Eq. (1) is a second-order differential equation with a variable, spatially dependent coefficient.

Nevertheless, the Poisson Eq. (1) can be solved analytically if we further assume that the radial ξ dependence for $\varepsilon(\mathbf{r})$ corresponds to the steplike model, as shown in Fig. 1. The dielectric constants for the prolate spheroid and the surrounding medium are ε_i and ε_o, respectively. The point charge e_s is assumed to be located, without loss of generality, at the point $\mathbf{r}_s=(\xi_s,\eta_s,\phi_s=0)$ in the xz plane inside or outside the dielectric spheroid defined by the equation $\xi=\xi_b$.

The interfocal distance of the prolate spheroid is a.

The analytical solution to this electrostatic problem has been published in the literature. In particular, the exact solution corresponding to the case that the point charge is set outside the prolate sphere is given in Ref. [20], while that corresponding to the case that the point charge is set inside the prolate sphere is given in Ref. [10]. We review these results here for the paper to be self-contained. In short, the electrostatic potential Φ_o or Φ_i at an observation point $\mathbf{r}=(\xi,\eta,\phi)$ outside or inside the spheroid, respectively, due to a point charge e_s inside the prolate spheroid (so $\xi_b>\xi_s\geq 1$) is given by

$$\Phi_o(\mathbf{r},\mathbf{r}_s)=\frac{e_s}{\varepsilon_i a}\sum_{n=0}^{\infty}\sum_{m=0}^{n}\varepsilon_i\mathcal{H}^P_{mn}\Delta_{mn}K^{-1}_{mn}Q^m_n(\xi)Y^m_n(\phi,\eta), \tag{2a}$$

$$\Phi_i(\mathbf{r},\mathbf{r}_s)=\frac{e_s}{\varepsilon_i|\mathbf{r}-\mathbf{r}_s|}+\frac{e_s}{\varepsilon_i a}\sum_{n=0}^{\infty}\sum_{m=0}^{n}(\varepsilon_i-\varepsilon_o)\mathcal{H}^P_{mn}\times Q^m_n(\xi_b)\hat{Q}^m_n(\xi_b)K^{-1}_{mn}P^m_n(\xi)Y^m_n(\phi,\eta), \tag{2b}$$

where $P^m_n(\ldots)$ and $Q^m_n(\ldots)$ are the associated Legendre functions of the first and second kinds, respectively, and

$$Y^m_n(\phi,\eta)=\cos(m\phi)P^m_n(\eta),$$

$$\mathcal{H}_{mn}=2(2n+1)(2-\delta_{m0})(-1)^m\left[\frac{(n-m)!}{(n+m)!}\right]^2,$$

$$\mathcal{H}^P_{mn}=\mathcal{H}_{mn}P^m_n(\xi_s)P^m_n(\eta_s),$$

$$\mathcal{H}^Q_{mn}=\mathcal{H}_{mn}Q^m_n(\xi_s)P^m_n(\eta_s),$$

$$\Delta_{mn}=P^m_n(\xi_b)\hat{Q}^m_n(\xi_b)-Q^m_n(\xi_b)\hat{P}^m_n(\xi_b),$$

$$K_{mn}=\varepsilon_o P^m_n(\xi_b)\hat{Q}^m_n(\xi_b)-\varepsilon_i Q^m_n(\xi_b)\hat{P}^m_n(\xi_b).$$

Here δ_{m0} is the Kronecker delta, and

$$\hat{P}^m_n(\xi)=(n-m+1)P^m_{n+1}(\xi)-(n+1)\xi P^m_n(\xi),$$

$$\hat{Q}^m_n(\xi)=(n-m+1)Q^m_{n+1}(\xi)-(n+1)\xi Q^m_n(\xi).$$

On the other hand, if the charge e_s is located at the point $\mathbf{r}_s=(\xi_s,\eta_s,\phi_s=0)$ outside the prolate sphere (so $\xi_s\geq\xi_b>1$), we have

$$\Phi_o(\mathbf{r},\mathbf{r}_s)=\frac{e_s}{\varepsilon_o|\mathbf{r}-\mathbf{r}_s|}+\frac{e_s}{\varepsilon_o a}\sum_{n=0}^{\infty}\sum_{m=0}^{n}(\varepsilon_i-\varepsilon_o)\mathcal{H}^Q_{mn}\times P^m_n(\xi_b)\hat{P}^m_n(\xi_b)K^{-1}_{mn}Q^m_n(\xi)Y^m_n(\phi,\eta), \tag{3a}$$

$$\Phi_i(\mathbf{r},\mathbf{r}_s)=\frac{e_s}{\varepsilon_o a}\sum_{n=0}^{\infty}\sum_{m=0}^{n}\varepsilon_o\mathcal{H}^Q_{mn}\Delta_{mn}K^{-1}_{mn}P^m_n(\xi)Y^m_n(\phi,\eta). \tag{3b}$$

From Eqs. (2) and (3), the self-polarization energy $V_s(\mathbf{r})$ can be calculated from $V_c(\mathbf{r},\mathbf{r}_s)$ by taking $\mathbf{r}=\mathbf{r}_s$, $e=e_s$, excluding the direct Coulomb interaction from $\Phi(\mathbf{r},\mathbf{r}_s)$, and dividing by 2 as it corresponds to a self-energy, namely, $V_s(\mathbf{r})=\frac{1}{2}e\Phi(\mathbf{r},\mathbf{r})$. Thus we get

$$V_s(\mathbf{r})=\begin{cases}\dfrac{e^2}{2\varepsilon_o a}\displaystyle\sum_{n=0}^{\infty}\sum_{m=0}^{n}(\varepsilon_i-\varepsilon_o)\mathcal{H}_{mn}P^m_n(\xi_b)\hat{P}^m_n(\xi_b)K^{-1}_{mn}Q^{m2}_n(\xi)P^{m2}_n(\eta), & \text{if } \xi\geq\xi_b,\\ \dfrac{e^2}{2\varepsilon_i a}\displaystyle\sum_{n=0}^{\infty}\sum_{m=0}^{n}(\varepsilon_i-\varepsilon_o)\mathcal{H}_{mn}Q^m_n(\xi_b)\hat{Q}^m_n(\xi_b)K^{-1}_{mn}P^{m2}_n(\xi)P^{m2}_n(\eta), & \text{if } \xi<\xi_b.\end{cases} \tag{4}$$

III. ANALYTICAL SOLUTION FOR THE QUASI-HARMONIC DIELECTRIC MODEL

The major problem of employing the simple steplike model and the corresponding analytical solution (4) to calculate the self-polarization energy lies in the fact that it diverges at the spheroidal surface $\xi=\xi_b$. In order to remove both the mathematical singularity and the unphysical assumption of the sharp transition in the dielectric constant at this surface, an intuitive way is to introduce a thin translation layer of finite width in the ξ direction, say 2δ, centered at $\xi=\xi_b$ with a continuous radial dielectric profile, say $\varepsilon(\xi)$, separating the two dielectric continua, leading to a three-layer dielectric model, as shown in Fig. 2. What should be emphasized is that, unlike the three-dielectric-layer model for the spherical geometry [19] in which the translation layer has the same physical width in the radial direction (r direction), the three-layer dielectric model proposed here for the spheroidal geometry uses a ξ-dependent width. As can be seen from Fig. 2, the actual width of the translation layer in the r direction is therefore not uniform. For the inner layer of $\xi\leq\xi_b-\delta$ (well inside the cavity), the dielectric constant takes the cavity value ε_i, while for the outer layer of $\xi\geq\xi_b+\delta$ (well outside the cavity), the dielectric constant takes the surrounding medium value ε_o. Between them, for the intermediate translation layer of $\xi_b-\delta<\xi<\xi_b+\delta$, one can choose any analytical and physically plausible continuous profile for $\varepsilon(\xi)$ to connect these two extreme values. Two natural

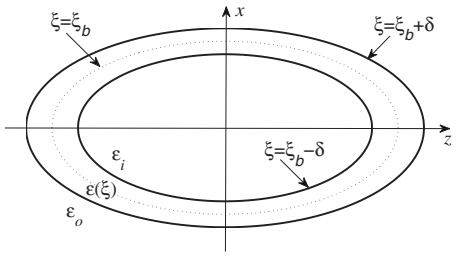

FIG. 2. Schematic illustration of a three-layer dielectric model: The inner layer ($\xi \leq \xi_b - \delta$) has a dielectric constant of ε_i, while the outer layer ($\xi \geq \xi_b + \delta$) has a dielectric constant of ε_o. The intermediate translation layer ($\xi_b - \delta < \xi < \xi_b + \delta$) assumes a continuous dielectric permittivity profile $\varepsilon(\xi)$ that connects ε_i and ε_o.

choices of $\varepsilon(\xi)$ include the linear profile defined by

$$\varepsilon(\xi) = \begin{cases} \varepsilon_i, & \text{if } \xi \leq \xi_I, \\ \dfrac{\varepsilon_i + \varepsilon_o}{2} + \dfrac{\varepsilon_i - \varepsilon_o}{2\delta}(\xi_b - \xi), & \text{if } \xi_I < \xi < \xi_O, \\ \varepsilon_o, & \text{if } \xi \geq \xi_O, \end{cases} \tag{5}$$

and the cosinelike profile given by

$$\varepsilon(\xi) = \begin{cases} \varepsilon_i, & \text{if } \xi \leq \xi_I, \\ \dfrac{\varepsilon_i + \varepsilon_o}{2} + \dfrac{\varepsilon_i - \varepsilon_o}{2}\cos\left(\dfrac{\xi - \xi_I}{2\delta}\pi\right), & \text{if } \xi_I < \xi < \xi_O, \\ \varepsilon_o, & \text{if } \xi \geq \xi_O, \end{cases} \tag{6}$$

respectively, where $\xi_I = \xi_b - \delta$ and $\xi_O = \xi_b + \delta$ represent the inner and the outer boundaries (edges) of the intermediate translation layer, respectively.

As indicated earlier, for a general dielectric permittivity profile $\varepsilon(\xi)$, it may be infeasible to find the analytical solution of the Poisson Eq. (1) since it is a second-order differential equation with a variable coefficient. When the permittivity assumes a continuous three-layer model and the radial dielectric profile in the translation layer is smooth, by following a procedure as described in Refs. [19,21,22] for finding analytical solutions to the Poisson equation with the spherical geometry, in principle it may be possible to obtain the analytical solution to the Poisson Eq. (1) with the spheroidal geometry as well. However, the procedure shall be quite complicated and thus expected to be inefficient for computations because it will involve the solution of a system of some auxiliary second-order differential equations with variable coefficients.

The Poisson Eq. (1) corresponding to a continuous three-layer dielectric model could also be solved numerically by the following procedure, which is very similar to that proposed by Bolcatto *et al.* in Ref. [16] for calculating self-polarization energies of spherical quantum dots. First, the translation layer of width 2δ (in terms of ξ) is subdivided into multiple regions, $[\xi_{l-1}, \xi_l]$, $l = 1, 2, \ldots, L-1$, with $\xi_0 = \xi_b - \delta$ and $\xi_{L-1} = \xi_b + \delta$, and in each one of them the select dielectric function is approximated by a constant value such as the mean value of the dielectric function in this region. As the result, the original continuous radial dielectric profile is approximated by a multistep (piecewise constant) one, and consequently, the original Poisson equation with the continuous radial dielectric profile reduces to one for layered dielectric prolate spheroids. By exploiting the analytical solution of the aforementioned steplike model, the solution of the Poisson equation for layered dielectric spheroids could be found in the same way as for layered spheres [16,18,21,23–25]. Indeed, this idea or similar has been used to calculate the potential distribution in a layered anisotropic spheroidal volume conductor [26]. However, this approach has a fundamental limitation: as its numerical nature requires the discretization of a continuous radial dielectric function $\varepsilon(\xi)$ into a piecewise constant one within the translation layer, new numerical divergence emerges. No matter how many steps are used to discretize the translation layer, the ultimate effect of this multistep approximation of a continuous radial dielectric profile $\varepsilon(\xi)$ is to approximate a continuous self-polarization energy by one with divergence at every step edge. We therefore believe that for a general continuous dielectric function, this procedure does not necessarily converge, let alone is able to recover the exact solution of the corresponding Poisson equation when $L \to \infty$.

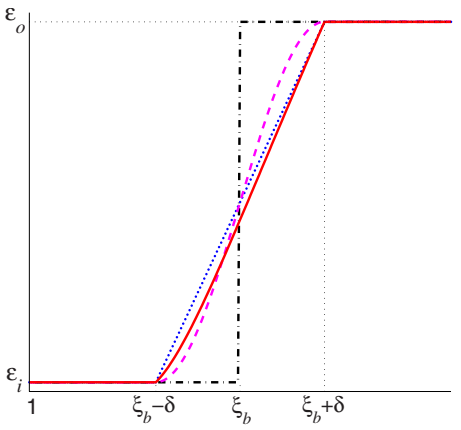

FIG. 3. (Color online) Illustration of several dielectric models for the translation layer between $\xi_b - \delta$ and $\xi_b + \delta$, assuming $\varepsilon_i < \varepsilon_o$. Dot-dashed line, the steplike model; dotted line, the linear model; dashed line, the cosinelike model; and solid line, the quasiharmonic model.

In this paper, aiming to overcome the mathematical divergence of the steplike model, instead we propose the following three-layer dielectric permittivity profile:

$$\varepsilon(\xi) = \begin{cases} \varepsilon_i, & \text{if } \xi \leq \xi_I, \\ \left[\alpha + \dfrac{\beta}{2}\ln\left(\dfrac{\xi+1}{\xi-1}\right)\right]^2, & \text{if } \xi_I < \xi < \xi_O, \\ \varepsilon_o, & \text{if } \xi \geq \xi_O, \end{cases} \tag{7}$$

where

$$\alpha = \frac{c_1\sqrt{\varepsilon_o} - c_2\sqrt{\varepsilon_i}}{c_1 - c_2}, \quad \beta = \frac{\sqrt{\varepsilon_i} - \sqrt{\varepsilon_o}}{c_1 - c_2},$$

with

$$c_1 = \frac{1}{2}\ln\left(\frac{\xi_I + 1}{\xi_I - 1}\right), \quad c_2 = \frac{1}{2}\ln\left(\frac{\xi_O + 1}{\xi_O - 1}\right).$$

For convenience, here and in the sequel, the dielectric permittivity profile in the translation layer given by Eq. (7) is referred to as the *quasiharmonic* profile since, although originally it was constructed through two harmonic functions $P_0^0(\xi) \equiv 1$ and $Q_0^0(\xi) = \frac{1}{2}\ln[(\xi+1)/(\xi-1)]$, it is not harmonic by itself. The three three-layer dielectric models mentioned so far together with the steplike model are illustrated in Fig. 3. As can be seen, like the linear profile, the derivative of the quasiharmonic dielectric profile is discontinuous at both edges of the translation layer, whereas the cosinelike dielectric profile is smooth at the same locations.

The analytical solution to the Poisson Eq. (1) corresponding to this quasiharmonic dielectric model is easy to find. Without loss of generality, let us first assume that a point charge e_s is located at the point $\mathbf{r}_s = (\xi_s, \eta_s, \phi_s = 0)$ in the xz plane inside the inner layer ($\xi_s \le \xi_I = \xi_b - \delta$). Accordingly, the Poisson Eq. (1) becomes

$$\nabla \cdot \varepsilon_i \nabla \Phi_i(\mathbf{r}, \mathbf{r}_s) = -4\pi e_s \delta(\mathbf{r} - \mathbf{r}_s), \quad \text{if } \xi \le \xi_I, \tag{8a}$$

$$\nabla \cdot \varepsilon(\xi) \nabla \Phi_t(\mathbf{r}, \mathbf{r}_s) = 0, \quad \text{if } \xi_I < \xi < \xi_O, \tag{8b}$$

$$\Delta \Phi_o(\mathbf{r}, \mathbf{r}_s) = 0, \quad \text{if } \xi \ge \xi_O, \tag{8c}$$

where Φ_i, Φ_t, and Φ_o stand for the electrostatic potential in the inner, the translation, and the outer layers, respectively.

At the two edges of the dielectric translation layer, the continuity of the potential and the normal flux requires that

$$\Phi_i|_{\xi=\xi_I} = \Phi_t|_{\xi=\xi_I}, \quad \left.\frac{\partial \Phi_i}{\partial \xi}\right|_{\xi=\xi_I} = \left.\frac{\partial \Phi_t}{\partial \xi}\right|_{\xi=\xi_I}, \tag{9a}$$

$$\Phi_o|_{\xi=\xi_O} = \Phi_t|_{\xi=\xi_O}, \quad \left.\frac{\partial \Phi_o}{\partial \xi}\right|_{\xi=\xi_O} = \left.\frac{\partial \Phi_t}{\partial \xi}\right|_{\xi=\xi_O}. \tag{9b}$$

The key in obtaining the analytical solution for the proposed quasiharmonic model is this important observation [19]: if $\varepsilon(\mathbf{r})$ in the quasiharmonic equation $\nabla \cdot [\varepsilon(\mathbf{r}) \nabla \phi(\mathbf{r})] = 0$ satisfies $\Delta \sqrt{\varepsilon(\mathbf{r})} = 0$, then $\Delta[\sqrt{\varepsilon(\mathbf{r})}\phi(\mathbf{r})] = 0$. Similarly, if $\varepsilon(\mathbf{r})$ in the quasielliptic equation $\nabla \cdot [\varepsilon(\mathbf{r}) \nabla \phi(\mathbf{r})] = \rho(\mathbf{r})$ satisfies $\Delta \sqrt{\varepsilon(\mathbf{r})} = 0$, then $\Delta[\sqrt{\varepsilon(\mathbf{r})}\phi(\mathbf{r})] = \rho(\mathbf{r})/\sqrt{\varepsilon(\mathbf{r})}$. Since by construction, $\Delta \sqrt{\varepsilon(\xi)} = 0$ in the translation layer, the potential in this layer Φ_t can thus be expressed as

$$\Phi_t(\mathbf{r}, \mathbf{r}_s) = \frac{e_s}{\sqrt{\varepsilon(\xi)}} \sum_{n=0}^{\infty} \sum_{m=0}^{n} [C_{mn} P_n^m(\xi) + D_{mn} Q_n^m(\xi)] Y_n^m(\phi, \eta),$$

or, when the charge e_s is located inside the translation layer, as

$$\Phi_t(\mathbf{r}, \mathbf{r}_s) = \frac{e_s}{\sqrt{\varepsilon_s \varepsilon(\xi)}|\mathbf{r} - \mathbf{r}_s|} + \frac{e_s}{\sqrt{\varepsilon(\xi)}} \sum_{n=0}^{\infty} \sum_{m=0}^{n} [C_{mn} P_n^m(\xi) + D_{mn} Q_n^m(\xi)] Y_n^m(\phi, \eta),$$

where $\varepsilon_s = \varepsilon(\xi_s)$, and C_{mn} and D_{mn} are undetermined constant expansion coefficients.

For the purpose of simplifying the mathematical formulations, now we actually write the potential in the three layers as

$$\Phi_o(\mathbf{r}, \mathbf{r}_s) = \frac{e_s}{\sqrt{\varepsilon_i \varepsilon_o} a} \sum_{n=0}^{\infty} \sum_{m=0}^{n} \mathcal{H}_{mn}^P A_{mn}^{(1)} Q_n^m(\xi) Y_n^m(\phi, \eta), \tag{10a}$$

$$\Phi_i(\mathbf{r}, \mathbf{r}_s) = \frac{e_s}{\varepsilon_i |\mathbf{r} - \mathbf{r}_s|} + \frac{e_s}{\varepsilon_i a} \sum_{n=0}^{\infty} \sum_{m=0}^{n} \mathcal{H}_{mn}^P B_{mn}^{(1)} P_n^m(\xi) Y_n^m(\phi, \eta), \tag{10b}$$

$$\Phi_t(\mathbf{r}, \mathbf{r}_s) = \frac{e_s}{\sqrt{\varepsilon_i \varepsilon(\xi)} a} \sum_{n=0}^{\infty} \sum_{m=0}^{n} \mathcal{H}_{mn}^P [C_{mn}^{(1)} P_n^m(\xi) + D_{mn}^{(1)} Q_n^m(\xi)] Y_n^m(\phi, \eta). \tag{10c}$$

Here, the constant expansion coefficients $A_{mn}^{(1)}$, $B_{mn}^{(1)}$, $C_{mn}^{(1)}$, and $D_{mn}^{(1)}$ can be determined by the boundary condition (9), together with the orthogonality of $\cos(m\phi)$ and that of the Legendre polynomial functions $P_n^m(\ldots)$, as well as the known expansion of the reciprocal distance in the prolate spheroidal coordinates [27–29], namely,

$$\frac{1}{|\mathbf{r} - \mathbf{r}_s|} = \begin{cases} \dfrac{1}{a} \displaystyle\sum_{n=0}^{\infty} \sum_{m=0}^{n} \mathcal{H}_{mn}^P Q_n^m(\xi) Y_n^m(\phi, \eta), & \text{if } \xi \ge \xi_s, \\ \dfrac{1}{a} \displaystyle\sum_{n=0}^{\infty} \sum_{m=0}^{n} \mathcal{H}_{mn}^Q P_n^m(\xi) Y_n^m(\phi, \eta), & \text{if } \xi \le \xi_s. \end{cases}$$

Omitting all details, for $n = 0, 1, \cdots$, and $m = 0, 1, \cdots, n$, we have

$$\mathbf{M} \times \begin{pmatrix} A_{mn}^{(1)} \\ B_{mn}^{(1)} \\ C_{mn}^{(1)} \\ D_{mn}^{(1)} \end{pmatrix} = \begin{pmatrix} -Q_n^m(\xi_I) \\ 0 \\ -\hat{Q}_n^m(\xi_I) \\ 0 \end{pmatrix},$$

where

$$\mathbf{M} = \begin{bmatrix} 0, & P_n^m(\xi_I), & -P_n^m(\xi_I), & -Q_n^m(\xi_I) \\ Q_n^m(\xi_O), & 0, & -P_n^m(\xi_O), & -Q_n^m(\xi_O) \\ 0, & \hat{P}_n^m(\xi_I), & -\hat{P}_n^m(\xi_I) - \frac{\beta}{\sqrt{\varepsilon_i}} P_n^m(\xi_I), & -\hat{Q}_n^m(\xi_I) - \frac{\beta}{\sqrt{\varepsilon_i}} Q_n^m(\xi_I) \\ \hat{Q}_n^m(\xi_O), & 0, & -\hat{P}_n^m(\xi_O) - \frac{\beta}{\sqrt{\varepsilon_o}} P_n^m(\xi_O), & -\hat{Q}_n^m(\xi_O) - \frac{\beta}{\sqrt{\varepsilon_o}} Q_n^m(\xi_O) \end{bmatrix}.$$

Similarly, if e_s is located inside the outer layer ($\xi_s \geq \xi_O = \xi_b + \delta$), we can write

$$\Phi_o(\mathbf{r}, \mathbf{r}_s) = \frac{e_s}{\varepsilon_o |\mathbf{r} - \mathbf{r}_s|} + \frac{e_s}{\varepsilon_o a} \sum_{n=0}^{\infty} \sum_{m=0}^{n} \mathcal{H}_{mn}^Q A_{mn}^{(2)} Q_n^m(\xi) Y_n^m(\phi, \eta), \tag{11a}$$

$$\Phi_i(\mathbf{r}, \mathbf{r}_s) = \frac{e_s}{\sqrt{\varepsilon_o \varepsilon_i} a} \sum_{n=0}^{\infty} \sum_{m=0}^{n} \mathcal{H}_{mn}^Q B_{mn}^{(2)} P_n^m(\xi) Y_n^m(\phi, \eta), \tag{11b}$$

$$\Phi_t(\mathbf{r}, \mathbf{r}_s) = \frac{e_s}{\sqrt{\varepsilon_o \varepsilon(\xi)} a} \sum_{n=0}^{\infty} \sum_{m=0}^{n} \mathcal{H}_{mn}^Q [C_{mn}^{(2)} P_n^m(\xi) + D_{mn}^{(2)} Q_n^m(\xi)] Y_n^m(\phi, \eta), \tag{11c}$$

where the constant expansion coefficients $A_{mn}^{(2)}$, $B_{mn}^{(2)}$, $C_{mn}^{(2)}$, and $D_{mn}^{(2)}$ can be calculated by

$$\mathbf{M} \times \begin{pmatrix} A_{mn}^{(2)} \\ B_{mn}^{(2)} \\ C_{mn}^{(2)} \\ D_{mn}^{(2)} \end{pmatrix} = \begin{pmatrix} 0 \\ -P_n^m(\xi_O) \\ 0 \\ -\hat{P}_n^m(\xi_O) \end{pmatrix}.$$

Finally, when e_s is located inside the intermediate layer ($\xi_I < \xi_s < \xi_O$), we can write

$$\Phi_o(\mathbf{r}, \mathbf{r}_s) = \frac{e_s}{\sqrt{\varepsilon_s \varepsilon_o} a} \sum_{n=0}^{\infty} \sum_{m=0}^{n} [\mathcal{H}_{mn}^Q A_{mn}^{(3)} + \mathcal{H}_{mn}^P A_{mn}^{(4)}] Q_n^m(\xi) Y_n^m(\phi, \eta), \tag{12a}$$

$$\Phi_i(\mathbf{r}, \mathbf{r}_s) = \frac{e_s}{\sqrt{\varepsilon_s \varepsilon_i} a} \sum_{n=0}^{\infty} \sum_{m=0}^{n} [\mathcal{H}_{mn}^Q B_{mn}^{(3)} + \mathcal{H}_{mn}^P B_{mn}^{(4)}] P_n^m(\xi) Y_n^m(\phi, \eta), \tag{12b}$$

$$\Phi_t(\mathbf{r}, \mathbf{r}_s) = \frac{e_s}{\sqrt{\varepsilon_s \varepsilon(\xi)} |\mathbf{r} - \mathbf{r}_s|} + \frac{e_s}{\sqrt{\varepsilon_s \varepsilon(\xi)} a} \sum_{n=0}^{\infty} \sum_{m=0}^{n} [(\mathcal{H}_{mn}^Q C_{mn}^{(3)} + \mathcal{H}_{mn}^P C_{mn}^{(4)}) P_n^m(\xi) + (\mathcal{H}_{mn}^Q D_{mn}^{(3)} + \mathcal{H}_{mn}^P D_{mn}^{(4)}) Q_n^m(\xi)] Y_n^m(\phi, \eta). \tag{12c}$$

Here, the constant expansion coefficients $A_{mn}^{(3)}$, $B_{mn}^{(3)}$, $C_{mn}^{(3)}$, and $D_{mn}^{(3)}$ are determined by

$$\mathbf{M} \times \begin{pmatrix} A_{mn}^{(3)} \\ B_{mn}^{(3)} \\ C_{mn}^{(3)} \\ D_{mn}^{(3)} \end{pmatrix} = \begin{pmatrix} P_n^m(\xi_I) \\ 0 \\ \hat{P}_n^m(\xi_I) + \frac{\beta}{\sqrt{\varepsilon_i}} P_n^m(\xi_I) \\ 0 \end{pmatrix},$$

while $A_{mn}^{(4)}$, $B_{mn}^{(4)}$, $C_{mn}^{(4)}$, and $D_{mn}^{(4)}$ are determined by

$$\mathbf{M} \times \begin{pmatrix} A_{mn}^{(4)} \\ B_{mn}^{(4)} \\ C_{mn}^{(4)} \\ D_{mn}^{(4)} \end{pmatrix} = \begin{pmatrix} 0 \\ Q_n^m(\xi_O) \\ 0 \\ \hat{Q}_n^m(\xi_O) + \frac{\beta}{\sqrt{\varepsilon_o}} Q_n^m(\xi_O) \end{pmatrix}.$$

The practical implementation of the above analytical solution additionally requires truncating the infinite summation at a finite n value, say N, which could be very large in order to reach convergence or high accuracy. In this case, to avoid overflow and potential computer cutoff errors when using Eqs. (10)–(12), we further carry out convenient rewritings of these equations. For convenience, for $n=0,1,\ldots$, and $m=0,1,\ldots,n$, we let

$$u_{mn}(\xi) = \frac{P_n^m(\xi)}{Q_n^m(\xi)}, \quad v_{mn}(\xi) = \frac{Q_n^m(\xi)}{P_n^m(\xi)}, \quad \gamma_{mn} = u_{mn}(\xi_I) v_{mn}(\xi_O),$$

and

$$\bar{P}_n^m(\xi) = \hat{P}_n^m(\xi)/P_n^m(\xi) = (n-m+1) P_{n+1}^m(\xi)/P_n^m(\xi) - (n+1)\xi,$$

$$\bar{Q}_n^m(\xi) = \hat{Q}_n^m(\xi)/Q_n^m(\xi) = (n-m+1) Q_{n+1}^m(\xi)/Q_n^m(\xi) - (n+1)\xi.$$

Then, when e_s is located inside the inner layer, we can write the potential in the three layers as

$$\Phi_o(\mathbf{r}, \mathbf{r}_s) = \frac{e_s}{\sqrt{\varepsilon_i \varepsilon_o} a} \sum_{n=0}^{\infty} \sum_{m=0}^{n} \mathcal{H}_{mn}^P A_{mn}^{(1)} Q_n^m(\xi) Y_n^m(\phi, \eta), \tag{13a}$$

$$\Phi_i(\mathbf{r},\mathbf{r}_s)=\frac{e_s}{\varepsilon_i|\mathbf{r}-\mathbf{r}_s|}+\frac{e_s}{\varepsilon_i a}\sum_{n=0}^{\infty}\sum_{m=0}^{n}\mathcal{H}_{mn}^{P}\upsilon_{mn}(\xi_I)B_{mn}^{(1)}P_n^m(\xi)Y_n^m(\phi,\eta), \tag{13b}$$

$$\Phi_t(\mathbf{r},\mathbf{r}_s)=\frac{e_s}{\sqrt{\varepsilon_i\varepsilon(\xi)}a}\sum_{n=0}^{\infty}\sum_{m=0}^{n}\mathcal{H}_{mn}^{P}[\upsilon_{mn}(\xi_O)C_{mn}^{(1)}P_n^m(\xi)+D_{mn}^{(1)}Q_n^m(\xi)]Y_n^m(\phi,\eta), \tag{13c}$$

where the expansion coefficients $A_{mn}^{(1)}$, $B_{mn}^{(1)}$, $C_{mn}^{(1)}$, and $D_{mn}^{(1)}$ are now calculated by

$$\mathbf{M}^{(1)}\times\begin{pmatrix}A_{mn}^{(1)}\\B_{mn}^{(1)}\\C_{mn}^{(1)}\\D_{mn}^{(1)}\end{pmatrix}=\begin{pmatrix}-1\\0\\-\bar{Q}_n^m(\xi_I)\\0\end{pmatrix},$$

with

$$\mathbf{M}^{(1)}=\begin{bmatrix}0, & 1, & -\gamma_{mn}, & -1\\ 1, & 0, & -1, & -1\\ 0, & \bar{P}_n^m(\xi_I), & \left(-\bar{P}_n^m(\xi_I)-\frac{\beta}{\sqrt{\varepsilon_i}}\right)\gamma_{mn}, & -\bar{Q}_n^m(\xi_I)-\frac{\beta}{\sqrt{\varepsilon_i}}\\ \bar{Q}_n^m(\xi_O), & 0, & -\bar{P}_n^m(\xi_O)-\frac{\beta}{\sqrt{\varepsilon_o}}, & -\bar{Q}_n^m(\xi_O)-\frac{\beta}{\sqrt{\varepsilon_o}}\end{bmatrix}.$$

Similarly, if e_s is located inside the outer layer, we can write

$$\Phi_o(\mathbf{r},\mathbf{r}_s)=\frac{e_s}{\varepsilon_o|\mathbf{r}-\mathbf{r}_s|}+\frac{e_s}{\varepsilon_o a}\sum_{n=0}^{\infty}\sum_{m=0}^{n}\mathcal{H}_{mn}^{Q}u_{mn}(\xi_O)A_{mn}^{(2)}Q_n^m(\xi)Y_n^m(\phi,\eta), \tag{14a}$$

$$\Phi_i(\mathbf{r},\mathbf{r}_s)=\frac{e_s}{\sqrt{\varepsilon_o\varepsilon_i}a}\sum_{n=0}^{\infty}\sum_{m=0}^{n}\mathcal{H}_{mn}^{Q}B_{mn}^{(2)}P_n^m(\xi)Y_n^m(\phi,\eta), \tag{14b}$$

$$\Phi_t(\mathbf{r},\mathbf{r}_s)=\frac{e_s}{\sqrt{\varepsilon_o\varepsilon(\xi)}a}\sum_{n=0}^{\infty}\sum_{m=0}^{n}\mathcal{H}_{mn}^{Q}[C_{mn}^{(2)}P_n^m(\xi)+u_{mn}(\xi_I)D_{mn}^{(2)}Q_n^m(\xi)]Y_n^m(\phi,\eta), \tag{14c}$$

where the expansion coefficients $A_{mn}^{(2)}$, $B_{mn}^{(2)}$, $C_{mn}^{(2)}$, and $D_{mn}^{(2)}$ are now determined by

$$\mathbf{M}^{(2)}\times\begin{pmatrix}A_{mn}^{(2)}\\B_{mn}^{(2)}\\C_{mn}^{(2)}\\D_{mn}^{(2)}\end{pmatrix}=\begin{pmatrix}0\\-1\\0\\-\bar{P}_n^m(\xi_O)\end{pmatrix},$$

with

$$\mathbf{M}^{(2)}=\begin{bmatrix}0, & 1, & -1, & -1\\ 1, & 0, & -1, & -\gamma_{mn}\\ 0, & \bar{P}_n^m(\xi_I), & -\bar{P}_n^m(\xi_I)-\frac{\beta}{\sqrt{\varepsilon_i}}, & -\bar{Q}_n^m(\xi_I)-\frac{\beta}{\sqrt{\varepsilon_i}}\\ \bar{Q}_n^m(\xi_O), & 0, & -\bar{P}_n^m(\xi_O)-\frac{\beta}{\sqrt{\varepsilon_o}}, & \left(-\bar{Q}_n^m(\xi_O)-\frac{\beta}{\sqrt{\varepsilon_o}}\right)\gamma_{mn}\end{bmatrix}.$$

Finally, when e_s is located inside the intermediate translation layer, we can write

$$\Phi_o(\mathbf{r},\mathbf{r}_s) = \frac{e_s}{\sqrt{\varepsilon_s\varepsilon_o}a}\sum_{n=0}^{\infty}\sum_{m=0}^{n}[\mathcal{H}_{mn}^{Q}u_{mn}(\xi_I)A_{mn}^{(3)} + \mathcal{H}_{mn}^{P}A_{mn}^{(4)}]Q_n^m(\xi)Y_n^m(\phi,\eta), \tag{15a}$$

$$\Phi_i(\mathbf{r},\mathbf{r}_s) = \frac{e_s}{\sqrt{\varepsilon_s\varepsilon_i}a}\sum_{n=0}^{\infty}\sum_{m=0}^{n}[\mathcal{H}_{mn}^{Q}B_{mn}^{(3)} + \mathcal{H}_{mn}^{P}v_{mn}(\xi_O)B_{mn}^{(4)}]P_n^m(\xi)Y_n^m(\phi,\eta), \tag{15b}$$

$$\Phi_t(\mathbf{r},\mathbf{r}_s) = \frac{e_s}{\sqrt{\varepsilon_s\varepsilon(\xi)}|\mathbf{r}-\mathbf{r}_s|} + \frac{e_s}{\sqrt{\varepsilon_s\varepsilon(\xi)}a}\sum_{n=0}^{\infty}\sum_{m=0}^{n}[(\mathcal{H}_{mn}^{Q}\gamma_{mn}C_{mn}^{(3)} + \mathcal{H}_{mn}^{P}v_{mn}(\xi_O)C_{mn}^{(4)})P_n^m(\xi)$$
$$+ (\mathcal{H}_{mn}^{Q}u_{mn}(\xi_I)D_{mn}^{(3)} + \mathcal{H}_{mn}^{P}\gamma_{mn}D_{mn}^{(4)})Q_n^m(\xi)]Y_n^m(\phi,\eta). \tag{15c}$$

Here, the expansion coefficients $A_{mn}^{(3)}$, $B_{mn}^{(3)}$, $C_{mn}^{(3)}$, and $D_{mn}^{(3)}$ are now determined by

$$\mathbf{M}^{(1)} \times \begin{pmatrix} A_{mn}^{(3)} \\ B_{mn}^{(3)} \\ C_{mn}^{(3)} \\ D_{mn}^{(3)} \end{pmatrix} = \begin{pmatrix} 1 \\ 0 \\ \bar{P}_n^m(\xi_I) + \dfrac{\beta}{\sqrt{\varepsilon_i}} \\ 0 \end{pmatrix},$$

while the expansion coefficients $A_{mn}^{(4)}$, $B_{mn}^{(4)}$, $C_{mn}^{(4)}$, and $D_{mn}^{(4)}$ are now determined by

$$\mathbf{M}^{(2)} \times \begin{pmatrix} A_{mn}^{(4)} \\ B_{mn}^{(4)} \\ C_{mn}^{(4)} \\ D_{mn}^{(4)} \end{pmatrix} = \begin{pmatrix} 0 \\ 1 \\ 0 \\ \bar{Q}_n^m(\xi_O) + \dfrac{\beta}{\sqrt{\varepsilon_o}} \end{pmatrix}.$$

Accordingly, from Eqs. (13)–(15), we can arrive at the self-polarization potential energy of a charged particle e at the location $\mathbf{r}$ as follows:

$$V_s(\mathbf{r}) = \begin{cases} \dfrac{e^2}{2\varepsilon_o a}\displaystyle\sum_{n=0}^{\infty}\sum_{m=0}^{n}\mathcal{H}_{mn}u_{mn}(\xi_O)A_{mn}^{(2)}Q_n^{m2}(\xi)P_n^{m2}(\eta), & \text{if } \xi \geq \xi_O, \\ \dfrac{e^2}{2\varepsilon_i a}\displaystyle\sum_{n=0}^{\infty}\sum_{m=0}^{n}\mathcal{H}_{mn}v_{mn}(\xi_I)B_{mn}^{(1)}P_n^{m2}(\xi)P_n^{m2}(\eta), & \text{if } \xi \leq \xi_I, \\ \dfrac{e^2}{2\varepsilon(\xi)a}\displaystyle\sum_{n=0}^{\infty}\sum_{m=0}^{n}\mathcal{H}_{mn}[\,\gamma_{mn}C_{mn}^{(3)}P_n^m(\xi)Q_n^m(\xi) + v_{mn}(\xi_O)C_{mn}^{(4)}P_n^{m2}(\xi) \\ \quad + u_{mn}(\xi_I)D_{mn}^{(3)}Q_n^{m2}(\xi) + \gamma_{mn}D_{mn}^{(4)}P_n^m(\xi)Q_n^m(\xi)\,]\,P_n^{m2}(\eta), & \text{if } \xi_I < \xi < \xi_O. \end{cases}$$

IV. EXTENSION TO OBLATE SPHEROIDAL CAVITIES

The results described in Secs. II and III can be readily extended to oblate spheroidal cavities if the corresponding oblate spheroidal coordinates (ξ,η,ϕ) are defined through

$$x = \frac{a}{2}\sqrt{(1+\xi^2)(1-\eta^2)}\cos\phi,$$

$$y = \frac{a}{2}\sqrt{(1+\xi^2)(1-\eta^2)}\sin\phi, \quad z = \frac{a}{2}\xi\eta,$$

where a is the interfocal distance of the oblate spheroid, $\xi \in [0,\infty)$ is the radial variable, $\eta \in [-1,1]$ is the angular variable, and $\phi \in [0,2\pi]$ is the azimuthal variable, respectively. Under this definition, the surface of constant ξ is an oblate spheroid with interfocal distance a. In particular, when $\xi=0$, the spheroid is degenerate and flattens to the circular disk in the plane $z=0$ with radius $a/2$. Then all the results obtained for prolate spheroids can be extended to oblate spheroids basically by following this rule: replace ξ by $i\xi$ where $i = \sqrt{-1}$ and $\mathcal{H}_{mn}$ by

$$\hat{\mathcal{H}}_{mn} = 2i(2n+1)(2-\delta_{m0})(-1)^m \left[\frac{(n-m)!}{(n+m)!}\right]^2.$$

As an example, a quasiharmonic three-layer dielectric permittivity profile is given by

$$\hat{\varepsilon}(\xi) = \varepsilon(i\xi) = \begin{cases} \varepsilon_i, & \text{if } \xi \le \xi_I, \\ \left[\alpha + \frac{\beta}{2}\ln\left(\frac{i\xi+1}{i\xi-1}\right)\right]^2, & \text{if } \xi_I < \xi < \xi_O, \\ \varepsilon_o, & \text{if } \xi \ge \xi_O, \end{cases} \tag{16}$$

where

$$\alpha = \frac{c_1\sqrt{\varepsilon_o} - c_2\sqrt{\varepsilon_i}}{c_1 - c_2}, \quad \beta = \frac{\sqrt{\varepsilon_i} - \sqrt{\varepsilon_o}}{c_1 - c_2},$$

with

$$c_1 = \frac{1}{2}\ln\left(\frac{i\xi_I+1}{i\xi_I-1}\right), \quad c_2 = \frac{1}{2}\ln\left(\frac{i\xi_O+1}{i\xi_O-1}\right).$$

Note that β is a pure imaginary number.

Then, when a charge e_s is located inside the inner layer, the potential in the three layers is given by

$$\Phi_o(\mathbf{r},\mathbf{r}_s) = \frac{e_s}{\sqrt{\varepsilon_i\varepsilon_o}a}\sum_{n=0}^{\infty}\sum_{m=0}^{n}\hat{\mathcal{H}}^P_{mn}\hat{A}^{(1)}_{mn}Q^m_n(i\xi)Y^m_n(\phi,\eta), \tag{17a}$$

$$\Phi_i(\mathbf{r},\mathbf{r}_s) = \frac{e_s}{\varepsilon_i|\mathbf{r}-\mathbf{r}_s|} + \frac{e_s}{\varepsilon_i a}\sum_{n=0}^{\infty}\sum_{m=0}^{n}\hat{\mathcal{H}}^P_{mn}v_{mn}(i\xi_I)\hat{B}^{(1)}_{mn}P^m_n(i\xi)Y^m_n(\phi,\eta), \tag{17b}$$

$$\Phi_t(\mathbf{r},\mathbf{r}_s) = \frac{e_s}{\sqrt{\varepsilon_i\hat{\varepsilon}(\xi)}a}\sum_{n=0}^{\infty}\sum_{m=0}^{n}\hat{\mathcal{H}}^P_{mn}[v_{mn}(i\xi_O)\hat{C}^{(1)}_{mn}P^m_n(i\xi) + \hat{D}^{(1)}_{mn}Q^m_n(i\xi)]Y^m_n(\phi,\eta), \tag{17c}$$

where the expansion coefficients $\hat{A}^{(1)}_{mn}$, $\hat{B}^{(1)}_{mn}$, $\hat{C}^{(1)}_{mn}$, and $\hat{D}^{(1)}_{mn}$ are calculated by

$$\hat{\mathbf{M}}^{(1)} \times \begin{pmatrix} \hat{A}^{(1)}_{mn} \\ \hat{B}^{(1)}_{mn} \\ \hat{C}^{(1)}_{mn} \\ \hat{D}^{(1)}_{mn} \end{pmatrix} = \begin{pmatrix} -1 \\ 0 \\ -\bar{Q}^m_n(i\xi_I) \\ 0 \end{pmatrix},$$

with

$$\hat{\mathbf{M}}^{(1)} = \begin{bmatrix} 0, & 1, & -\hat{\gamma}_{mn}, & -1 \\ 1, & 0, & -1 & -1 \\ 0, & \bar{P}^m_n(i\xi_I), & \left(-\bar{P}^m_n(i\xi_I) - \frac{\beta}{\sqrt{\varepsilon_i}}\right)\hat{\gamma}_{mn}, & -\bar{Q}^m_n(i\xi_I) - \frac{\beta}{\sqrt{\varepsilon_i}} \\ \bar{Q}^m_n(i\xi_O), & 0, & -\bar{P}^m_n(i\xi_O) - \frac{\beta}{\sqrt{\varepsilon_o}}, & -\bar{Q}^m_n(i\xi_O) - \frac{\beta}{\sqrt{\varepsilon_o}} \end{bmatrix},$$

and

$$\hat{\mathcal{H}}^P_{mn} = \hat{\mathcal{H}}_{mn}P^m_n(i\xi_s)P^m_n(\eta_s),$$

$$\hat{\gamma}_{mn} = u_{mn}(i\xi_I)v_{mn}(i\xi_O).$$

Note that, using the fact that

$$Q^0_0(i\xi) \equiv \frac{1}{2}\ln\left(\frac{i\xi+1}{i\xi-1}\right) = i\left(\tan^{-1}(\xi) - \frac{\pi}{2}\right),$$

the quasiharmonic three-layer dielectric model given by Eq. (16) can be rewritten as

$$\hat{\varepsilon}(\xi) = \begin{cases} \varepsilon_i, & \text{if } \xi \le \xi_I, \\ (\hat{\alpha} - \hat{\beta}\tan^{-1}\xi)^2, & \text{if } \xi_I < \xi < \xi_O, \\ \varepsilon_o, & \text{if } \xi \ge \xi_O, \end{cases} \tag{18}$$

where

$$\hat{\alpha} = \frac{\hat{c}_1\sqrt{\varepsilon_o} - \hat{c}_2\sqrt{\varepsilon_i}}{\hat{c}_1 - \hat{c}_2}, \quad \hat{\beta} = \frac{\sqrt{\varepsilon_o} - \sqrt{\varepsilon_i}}{\hat{c}_1 - \hat{c}_2},$$

with

$$\hat{c}_1 = \tan^{-1}(\xi_I), \quad \hat{c}_2 = \tan^{-1}(\xi_O).$$

In this form, $\hat{\beta}$ is a real number, and in fact $\hat{\beta} = -\beta i$ or $\beta = \hat{\beta}i$.

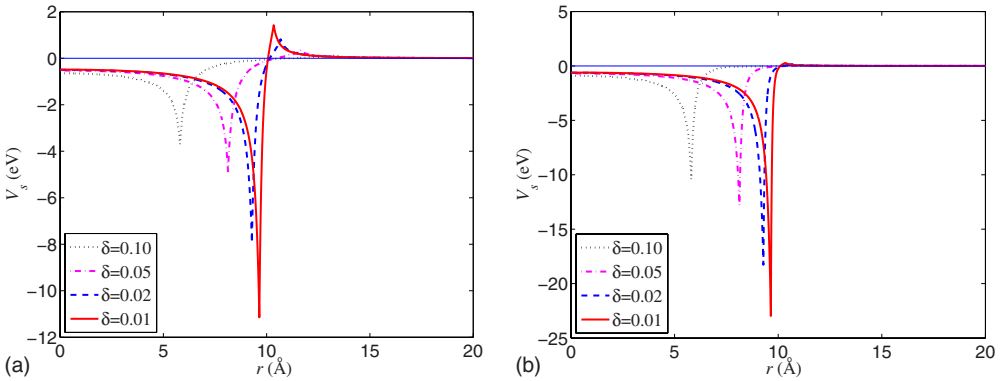

FIG. 4. (Color online) Self-polarization energy V_s along a minor axis of the prolate spheroid $(x^2+y^2)/10^2+z^2/20^2=1$ corresponding to the quasiharmonic model with $\delta=0.1$, 0.05, 0.02, and 0.01. (a) $\varepsilon_o=10$, and (b) $\varepsilon_o=80$.

V. NUMERICAL EXAMPLES

To illustrate the simulated behavior of the quasiharmonic dielectric model and the corresponding analytical solution for a prolate spheroid, we consider the dielectric prolate spheroid given by $(x^2+y^2)/a_1^2+z^2/a_2^2=1$ with $a_1=10$ Å and $a_2=20$ Å, which leads to $\xi_b \approx 1.1547$. The prolate spheroid has a low dielectric constant of $\varepsilon_i=2$, and is embedded in a dissimilar dielectric medium of a high dielectric constant of $\varepsilon_o=10$ or 80, respectively. In all numerical simulations, the imposed upper limit of n is set to $N=100$, and all analytical results and illustrative plots are based on the calculation of the self-polarization energies of 10 000 unit charges (in atomic unit) uniformly distributed (in terms of the ξ-dependent distance) either along a minor axis of the prolate spheroid or along the ray extending from the center to the point (10,0,20). Figure 4 shows the self-polarization energy V_s along a minor axis of the prolate spheroid, and Fig. 5 shows that along the ray pointing to the point (10,0,20), respectively, corresponding to the quasiharmonic model with $\delta=0.1$, 0.05, 0.02, and 0.01.

It is well known that under the steplike model, when the source charge is placed in the region with a lower dielectric constant, the induced charges have the opposite sign as the source charge and then the interaction between the source and the induced charges is attractive. On the contrary, if the source charge is located in the region with a higher dielectric constant, the induced charges have the same sign as the source charge and then the interaction is repulsive. As can be seen from Figs. 4 and 5, under the quasiharmonic model, the self-polarization energy remains negative inside the cavity, and the negative potential extends to the outside of the cavity to some extent. As the translation layer decreases in size, however, the self-polarization energy given by the analytical solution for the quasiharmonic model will reduce to that for the steplike model (not shown in the graphs). In addition, we can observe that the quasiharmonic dielectric model leads to singularity in the self-polarization potential energy at both edges of the translation layer, precisely where the derivative of $\varepsilon(\mathbf{r})$ is discontinuous.

Finally, we apply the proposed quasiharmonic dielectric model and the corresponding analytical solution to calculate the self-polarization energy of a prolate spheroidal quantum dot [16], in which the dielectric constant inside the dot is typically higher than that outside, and consequently, a repulsive (positive) self-polarization potential energy arises due to the mutual interaction between the (inside-dot) source and its own induced charges. Specifically, we consider a small prolate spheroidal quantum dot given by the same equation but with $\varepsilon_i=12.6$ (GaAs), and $\varepsilon_o=1$ (vacuum), respectively. Again in all calculations, the imposed upper limit of n used in the infinite summation is set to $N=100$, and in calculating self-polarization energies, all 10 000 charges are assumed to be unit charges (in atomic unit) and uniformly distributed (in

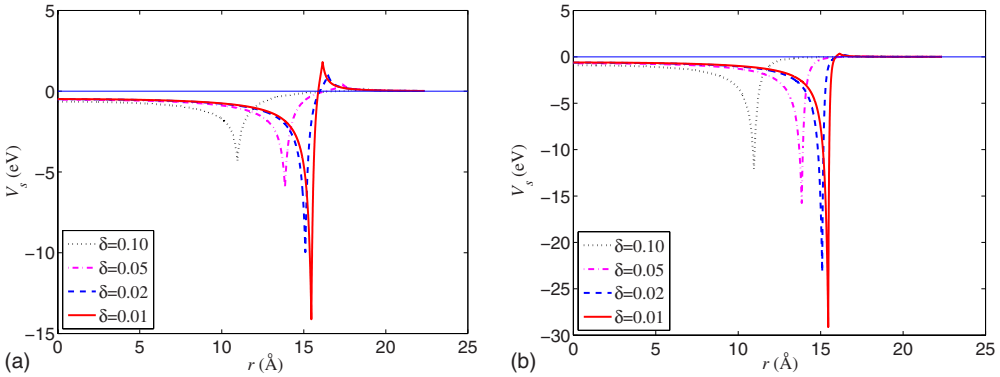

FIG. 5. (Color online) Self-polarization energy V_s along the ray extending from the center to the point (10,0,20) corresponding to the quasiharmonic model with $\delta=0.1$, 0.05, 0.02, and 0.01. (a) $\varepsilon_o=10$, and (b) $\varepsilon_o=80$.

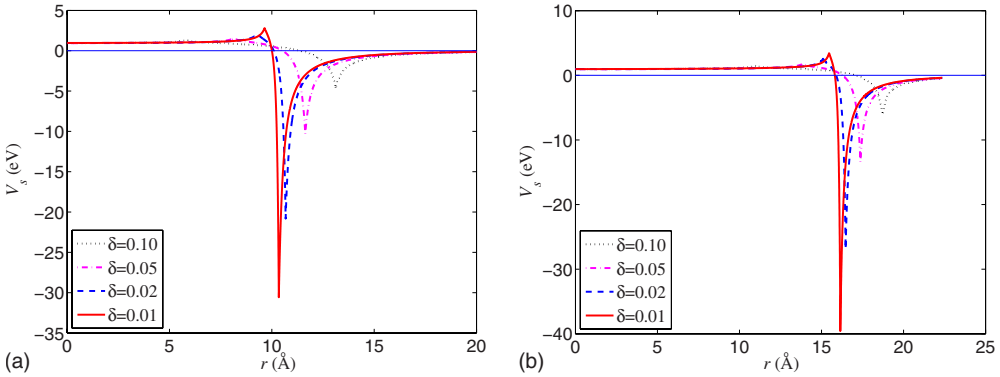

FIG. 6. (Color online) Self-polarization energy V_s of a prolate spheroidal quantum dot as a function of r corresponding to the quasiharmonic model with δ=0.1, 0.05, 0.02, and 0.01. (a) Along a minor axis of the prolate spheroid, and (b) along the ray extending from the center to the point (10,0,20).

terms of the ξ-dependent distance) along a line. Figure 6(a) shows the self-polarization energy V_s along a minor axis of the prolate spheroidal quantum dot, and Fig. 6(b) shows that along the ray extending from the center to the point (10,0,20), respectively, corresponding to the quasiharmonic model with δ=0.1, 0.05, 0.02, and 0.01.

As mentioned earlier, in all simulations presented in the present paper, the imposed upper limit of n used in the infinite summation is set to N=100. In Fig. 7, we plot the relative error E in the self-polarization energy defined as

$$E(\mathbf{r}) = \frac{|V_s^{(N)}(\mathbf{r}) - V_s^{(120)}(\mathbf{r})|}{\max\limits_{0\le r\le 20} |V_s^{(120)}(\mathbf{r})|}, \tag{19}$$

where $V_s^{(N)}(\mathbf{r})$ denotes the computed self-polarization energy by using the analytical series solution with a chosen upper limit N, for the case of Fig. 4(a) with δ=0.1. As can be seen, N=100 or even a smaller one like N=60 is far beyond the achievement of convergence (more precisely, the desired accuracy) if a charge is away from the two edges of the translation layer. But on the other hand, as is well known for this kind of problems, when a charge is close to the boundaries, the convergence of the series solution will be slow, requiring a great number of terms in the series expansion to achieve satisfactory accuracy in the solution. The closer the charge is to the boundaries, the greater the required number N is. Nonetheless, considering that a total of 10 000 uniformly distributed charges are used in the numerical calculations, we thus conclude that, mathematically, the series solution always converges regardless of charge location (but the convergence rate could be very slow if the charge is very close to a boundary). For example, the maximum relative error, which occurs at the closest sample point to the inner boundary, goes down approximately from 11% to 6% to 2% when the upper limit N goes up from 60 to 80 to 100. The same observations hold for all other cases presented in the paper. In particular, the maximum relative error with using N =100 among all these cases is about 5.66%, which happens for the case of Fig. 5(b) with δ=0.01. Moreover, the numerical experiments also indicate that, to achieve the same accuracy, a greater upper limit N is needed if the translation layer is thinner or the dielectric mismatch between the two underlying materials is larger. For examples, for the case of Fig. 4(a) where ε_i=2 and ε_o=10, the maximum relative error with using N=100 goes up from 2.44% to 2.74% to 2.97% to 3.62% when δ goes down from 0.1 to 0.05 to 0.02 to 0.01. And on the other hand, for the case of Fig. 4(b) where ε_i =2 and ε_o=80, the maximum relative error with using N =100 goes up from 3.48% to 3.54% to 4.35% to 5.08% when δ goes down from 0.1 to 0.05 to 0.02 to 0.01.

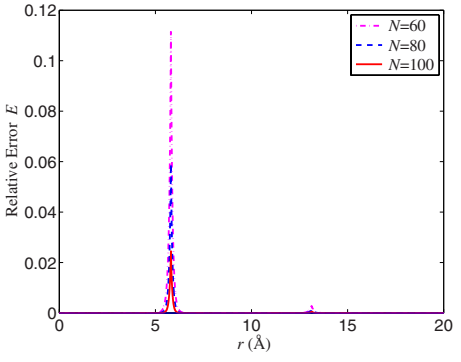

FIG. 7. (Color online) The relative error E in the self-polarization energy defined in Eq. (19) for the case of Fig. 4(a) with δ=0.1.

VI. CONCLUDING REMARKS

The novel three-dielectric-layer hybrid solvation model for treating electrostatic interactions in biomolecular simulations has been extended from the spherical geometry to the prolate/oblate spheroidal geometries. The corresponding series solutions for the generalized Coulomb potential and the self-polarization energy in terms of the associated Legendre functions have been presented. The proposed quasiharmonic dielectric model can overcome the inherent mathematical divergence in the self-polarization energy that exists in the simple steplike dielectric model, and can find its application in many other areas that involve the calculation of the generalized Coulomb potential, including the calculation of self-polarization energies of spheroidal quantum dots [16–18,25]. In addition, the model may also have potential applications

in the simulation of light scattering by inhomogeneous spheroidally symmetric particles.

Furthermore and more importantly, utilizing the analytical solution of the quasiharmonic dielectric model, we can develop a robust numerical method for solving the Poisson equation under any three-layer dielectric model that employs a smooth radial dielectric profile, such as the linear and the cosinelike models mentioned in Sec. III. The idea is very simple [30]. First we subdivide the translation layer, $\xi_b-\delta<\xi<\xi_b+\delta$, into multiple regions. Then, in each of them we approximate the select dielectric function by a quasiharmonic one. In this way the original continuous dielectric profile is approximated by a piecewise smooth but yet continuous one. Next, in each region the series solution of the Poisson equation can be written in terms of the associated Legendre functions. The whole solution will not exhibit any numerical divergence in the self-polarization energy at any interface between any two neighboring regions, an indispensable property that one cannot expect if the dielectric function in each region is approximated simply by a constant value [16]. Finally, by following the spirit of Refs. [21,23,30], namely, by using a procedure in analogy to the analysis of transmission lines, we shall be able to obtain recursive formulas for calculating those expansion coefficients in the series solutions. Due to page limit, we will investigate this approach in detail in a separate publication [31].

Finally, as pointed out before, the results can be straightforwardly extended to triaxial ellipsoidal cavities, which may be needed since, for example, realistic quantum dots might neither be perfect spheres nor be perfect spheroids. What makes it even more important is the fact that, among the 11 coordinate systems in which the Laplace equation (more precisely, the Helmholtz equation) is separable, the other ten coordinate systems can be considered as degenerate forms of the ellipsoidal one [27]. Generally speaking, to extend the results from the spheroidal geometry to the ellipsoidal one, the spheroidal harmonics are to be replaced by the ellipsoidal harmonics. In particular, the radial functions, which are the associated Legendre functions of the first and the second kinds $P_n^m(\xi)$ and $Q_n^m(\xi)$ under the prolate coordinate system, are now the Lamé functions of the first and the second kinds $E_n^p(\xi)$ and $F_n^p(\xi)$ [32–36]. Accordingly, a quasiharmonic three-layer dielectric permittivity profile can be defined by

$$\varepsilon(\xi)=\begin{cases}\varepsilon_i, & \text{if } \xi\le\xi_I,\\ [\alpha+\beta F_0^1(\xi)]^2, & \text{if } \xi_I<\xi<\xi_O,\\ \varepsilon_o, & \text{if } \xi\ge\xi_O,\end{cases} \tag{20}$$

where

$$\alpha=\frac{c_1\sqrt{\varepsilon_o}-c_2\sqrt{\varepsilon_i}}{c_1-c_2},\quad \beta=\frac{\sqrt{\varepsilon_i}-\sqrt{\varepsilon_o}}{c_1-c_2},$$

with

$$c_1=F_0^1(\xi_I),\quad c_2=F_0^1(\xi_O).$$

The analytical solution to the Poisson equation corresponding to this dielectric model can then be obtained in the same way as described in this paper, and the resulting formulations, although undoubtedly more elaborate and cumbersome, are expected to be very similar to those for the spheroidal geometry. However, again due to page limit, we will investigate this most general case in detail in a future publication.

ACKNOWLEDGMENTS

The authors thank the support of the National Natural Science Foundation of China (Grant No. 10971181) for the work reported in this paper. Additionally, the authors thank anonymous reviewers for their constructive suggestions that greatly improved this manuscript.

[1] P. Koehl, Curr. Opin. Struct. Biol. **16**, 142 (2006).
[2] R. M. Levy and E. Gallicchio, Annu. Rev. Phys. Chem. **49**, 531 (1998).
[3] C. Sagui and T. A. Darden, Annu. Rev. Biophys. Biomol. Struct. **28**, 155 (1999).
[4] M. Feig and C. L. Brooks III, Curr. Opin. Struct. Biol. **14**, 217 (2004).
[5] N. A. Baker, Curr. Opin. Struct. Biol. **15**, 137 (2005).
[6] A. Okur and C. Simmerling, in *Annual Reports in Computational Chemistry*, edited by D. C. Spellmeyer (Elsevier Science, Amsterdam, 2006), Vol. 2, Chap. 6, pp. 97–109.
[7] M. S. Lee, F. R. Salsbury, Jr., and M. A. Olson, J. Comput. Chem. **25**, 1967 (2004).
[8] M. S. Lee and M. A. Olson, J. Phys. Chem. B **109**, 5223 (2005).
[9] J. G. Kirkwood, J. Chem. Phys. **2**, 351 (1934).
[10] S. Deng, J. Electrost. **66**, 549 (2008).
[11] S. Deng, J. Electrost. **67**, 807 (2009).
[12] D. V. Redzic and S. S. Redzic, J. Phys. D **38**, 3991 (2005).
[13] F. Stern, Phys. Rev. B **17**, 5009 (1978).
[14] D. B. Tran Thoai, R. Zimmermann, M. Grundmann, and D. Bimberg, Phys. Rev. B **42**, 5906 (1990).
[15] L. Bányai, P. Gilliot, Y. Z. Hu, and S. W. Koch, Phys. Rev. B **45**, 14136 (1992).
[16] P. G. Bolcatto and C. R. Proetto, J. Phys.: Condens. Matter **13**, 319 (2001).
[17] P. G. Bolcatto and C. R. Proetto, Phys. Status Solidi **220**, 191 (2000).
[18] J. L. Movilla and J. Planelles, Comput. Phys. Commun. **170**, 144 (2005).
[19] P. Qin, Z. Xu, W. Cai, and D. Jacobs, Comm. Comp. Phys. **6**, 955 (2009).
[20] D. V. Redžić, Am. J. Phys. **62**, 1118 (1994).
[21] A. Sihvola and I. V. Lindell, J. Electromagn. Waves Appl. **3**, 37 (1989).
[22] A. Sihvola and I. V. Lindell, J. Electromagn. Waves Appl. **4**, 1 (1990).
[23] I. V. Lindell, M. E. Ermutlu, and A. Sihvola, IEE Proc. Micro-

waves, Antennas Propag. **139**, 186 (1992).
[24] A Sihvola and I. V. Lindell, J. Electromagn. Waves Appl. **2**, 741 (1988).
[25] J. L. Movilla and J. Planelles, Phys. Rev. B **71**, 075319 (2005).
[26] J. C. de Munck, J. Appl. Phys. **64**, 464 (1988).
[27] P. M. Morse and H. Feshbach, *Methods of Theoretical Physics* (McGraw-Hill, New York, 1953).
[28] E. W. Hobson, *The Theory of Spherical and Ellipsoidal Harmonics* (Cambridge University Press, Cambridge, England, 1931).
[29] W. R. Smythe, *Static and Dynamic Electricity*, 3rd ed. (Hemisphere, New York, 1989).
[30] S. Deng, Comput. Phys. Commun. (to be published).
[31] C. Xue and S. Deng, Comm. Comp. Phys. (to be published).
[32] T. Miloh, Isr. J. Technol. **11**, 63 (1973).
[33] J. W. Perram and P. J. Stiles, Proc. R. Soc. London, Ser. A **349**, 125 (1976).
[34] T. Miloh, J. Ship Res. **23**, 66 (1979).
[35] J. C. E. Sten, J. Electrost. **64**, 647 (2006).
[36] L. C. Lew Yan Voon and M. Willatzen, J. Phys.: Condens. Matter **16**, 1087 (2004).